International Journal of Materials Science

E-ISSN: 2707-823X
P-ISSN: 2707-8221
IJMS 2021; 2(2): 08-15
Received: 10-10-2021
Accepted: 20-11-2021

Shashank Sharma
Department of Physics, Kalinga University, Naya Raipur, Chhattisgarh, India

Sanjay Kumar Dubey
Department of Physics, Kalinga University, Naya Raipur, Chhattisgarh, India

AK Diwakar
Department of Physics, Kalinga University, Naya Raipur, Chhattisgarh, India

Corresponding Author:
Shashank Sharma
Department of Physics, Kalinga University, Naya Raipur, Chhattisgarh, India
Email: dr.shashankeinstein@rediffmail.com

Luminescence investigation on $Ca_2MgSi_2O_7:Eu^{2+}$, Dy^{3+} phosphor

Shashank Sharma, Sanjay Kumar Dubey and AK Diwakar

Abstract
$Ca_2MgSi_2O_7:Eu^{2+}$, Dy^{3+} phosphor was synthesized by combustion reaction technique. Phase Identification was done by X-ray diffraction analysis and its results revealed tetragonal, Akermanite structure with a space group $P\bar{4}2_1m$. This structure is a member of melilite group. The average crystallite size (D) is calculated as 30.77nm and lattice strain as 0.26. The functional group identification of this phosphor with the help of FTIR spectroscopy. When the $Ca_2MgSi_2O_7:Eu^{2+}$, Dy^{3+} phosphor was excited with 396nm wavelength single broad emission peak situated at 532nm was obtained. PL and CIE chromaticity diagram clearly indicates that the bright green emission was observed near UV region. Thermo-luminescence (TL) of the UV-irradiated (254 nm) samples was recorded with the help of routine TL set-up Nucleonix TLD reader with constant heating rate 5^0Cs^{-1}. The optimum TL intensity assigned at 110.78^0C temperature and displays single TL glow curve peak. The favorable features for applications likewise near UV-LED conversion phosphor, drug delivery, tissue engineering, bone material, detection of cancer, Image processing of computer science and found their considerable persistency etc. In this present paper, XRD, FTIR, PL, CIE Chromaticity Diagram, TL properties of the phosphor also reported.

Keywords: X-ray diffraction (XRD), Fourier Transform Infra-Red Spectroscopy (FTIR), Photoluminescence (PL), CIE Chromaticity Diagram, Thermo-luminescence (TL) and $Ca_2MgSi_2O_7:Eu^{2+}$, Dy^{3+}

1. Introduction
Basically, the occurrence of thermo-luminescence (TL) is related to the Thermally Stimulated process. In practice, it has been observed that TL is a light emission from a substance after removing of energy excited through the temperature provided for stimulation [1]. Matsuzawa *et al*. widely reported that blue, green and red long persistent $SrAl_2O_4:Eu^{2+}$, Dy^{3+} phosphor developed over the visible light region. This phosphor brightness and persistent time are not longer to applicable to practical overview [2]. It is generally agreed that Eu^{2+} is a most common emission centre in persistent phosphor hosted by the $4f7 \rightarrow 4f^65d^1$ transition [3-5]. Erkul Karacaogu *et al*. investigated that different rare earth doped $Ca_2MgSi_2O_7$ was prepared by solid-state reaction method under weak reduction atmosphere [6]. $Ca_2MgSi_2O_7$ have been broadly interesting from the manufacturing purpose because it is clearly indicating to better qualities of product sample, stability, energy consumed, because both calcium and silica are abundant and relatively inexpensive [7]. Silicates are highly chemical resistance and visible light transparency and hence they are attractive class of inorganic materials used for wide range of applications [3, 8]. Due to their high thermal, chemical stabilities, low cost, excellent water resistance and strong absorption in the near UV region [9]. Matsuzaua *et al*. proposed a "hole transfer model", which suggested that the Dy^{3+} acted as hole traps (Dy^{3+} + hole → Dy^{4+}), and Eu2+ acted as an electron traps (Eu^{2+} + e → Eu^+) [10]. The Dy^{3+} ions act as deep hole trap levels, which are located between the ground (low energy state) and excited (high energy state) states of Eu^{2+}. After stimulation by UV light, ground states of Eu^{2+} stimulation occurs as a result of electron and hole pairs generation from the ground state 4f to excited 4f5d state. Some free holes transported into the conduction band are captured by the Dy^{3+} traps [11]. Jiang *et al*. reported that the possible sites for incorporating Eu^{2+} in $Ca_2MgSi_2O_7$ lattice are Ca^{2+} sites, or the Mg^{2+} sites or the Si^{4+} sites, Mg^{2+} (0.58 Å) and Si^{4+} sites (0.26 Å) are small, but Ca^{2+} (1.12 Å) is equal to the size of Eu^{2+} (1.12 Å). So, Eu^{2+} ions hardly incorporate into tetrahedral [MgO_4] and [SiO_4] and only incorporate into [CaO_8] anions complexes in host [27].

Therefore, in the present work, we report the phosphor synthesis, structural characterization and luminescence properties of $Ca_2MgSi_2O_7:Eu^{2+}$, Dy^{3+} phosphor by combustion synthesis technique. Investigation on the crystal structure was determined by the X-ray diffraction (XRD) techniques. Luminescence properties were also investigated on the basis of FTIR, Photoluminescence (PL), CIE color coordinates as well as Thermo-luminescence (TL) has been studied in detail.

2. Experimental studies

2.1 Sample preparation

In our study, the prepared samples with stoichiometric ratio of $Ca_2MgSi_2O_7:Eu^{2+}$, Dy^{3+} were synthesized via conventional high-temperature combustion synthesis route. Initially, all raw reagents such as Ca $(NO_3)_2$ (99.99%), Mg $(NO_3)_2$ (99.99%), SiO_2*H_2O (99.99%) and H_3BO_3 (99.99%) of Hi-media (AR grade) and Eu $(NO_3)_3$ (99.99%) and Dy $(NO_3)_3$ (99.99%) were used. Very little amount of boric acid [H_3BO_3 (99.99%)] was used as a flux. Urea (NH_2CONH_2) used as a combustion fuel. The precursor powders were mixed thoroughly with the help of very little amount of acetone (CH_3COCH_3) for 2 hour before being transferred to a cylindrical silica crucible. Then the mixture was fired at 650 ^oC in muffle furnace. The entire combustion process was completed in about 5 min. The mixture undergoes thermal dehydration and ignites at 950 ^oC for 1h in a weak reducing atmosphere with liberation of gaseous products, to yield silicates. The weak reducing atmospheres are produced by using activated charcoal and the final product was obtained with applying additional grinding into a fine powder. The resulting sample was restored in airtight bottle for characterization studies.

The chemical reaction of this process is given as follows

$$Ca(NO_3)_2 + Mg(NO_3)_2 + SiO_2*H_2O + NH_2CONH_2 + Dy(NO_3)_3 + Eu(NO_3)_3 \rightarrow Ca_2MgSi_2O_7:Eu^{2+}, Dy^{3+} + H_2O(\uparrow) + CO_2(\uparrow) + N_2(\uparrow) \quad (1)$$

We have generally agreed, for any combustion process, fuel and oxidizers are required. Metal nitrates as oxidizers and urea is also employed as a fuel. Stoichiometric compositions of all metal nitrates and fuel are calculated based in propellant chemistry. Thus, the heat of combustion is maximum for Oxidizer/Fuel ratio 1 [12].

2.2 Sample characterization

XRD study of the crystalline structure, size and phase composition of the synthesized phosphor were noted with the help of Bruker D8 advance X-ray diffractometer with Cu-K_α radiation having wavelength (λ = 1.5406 Å, at 40 kV, 40 mA), respectively. Actual formation of this phosphor was obtained through FTIR. An FTIR spectrum was recorded with the help of Bruker Alpha Fourier transform Infra-red Spectroscopy. In photoluminescence spectra (PL), emission spectra were recorded by a spectro-fluorophotometer (SHIMADZU, RF-5301 PC) using a xenon lamp of power 150 watt as excitation source [13]. A routine Thermo-luminescence (TL) study of the UV-irradiated (254 nm) samples was recorded with the help of routine TL set-up Nucleonix TLD reader with constant heating rate 5 $^oCs^{-1}$ [14]. All experiments were performed in identical conditions and it was observed that the results were reproducible. All measurements recorded at the room temperature.

3. Results and Discussion

3.1 X-ray diffraction (XRD)

XRD patterns of $Ca_2MgSi_2O_7:Eu^{2+}$, Dy^{3+} phosphor synthesized by combustion route method is shown in Fig. 1. It is recorded in the range ($10^o \backslash 2\theta \backslash 80^o$). All the peaks show well agreement with the JCPDS No. 17-1149 [15]. The phase formation of the prepared phosphors was also confirmed by XRD characterization. The standard $Ca_2MgSi_2O_7$ structure, cell volume and lattice parameters are observed from data base code AMCSD 0008032 [16]. Table 1 shown calculation of all parameters showed of the phosphor. It is also observed that the influence of doping doesn't affect the phase structure of the phosphor.

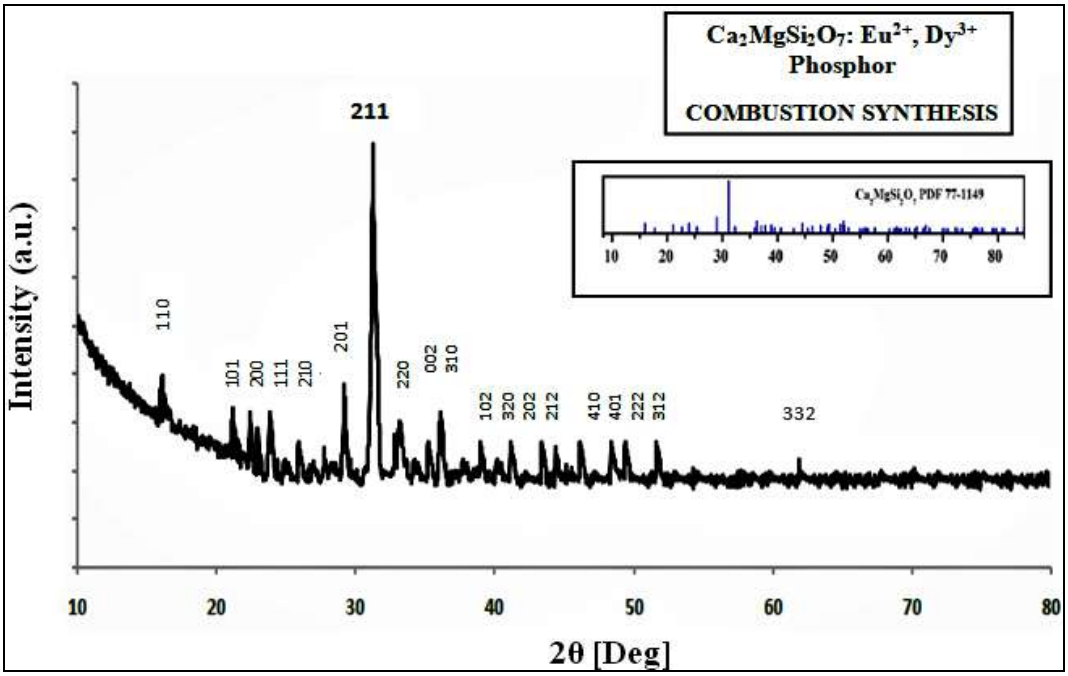

Fig 1: XRD pattern of $Ca_2MgSi_2O_7:Eu^{2+}$, Dy^{3+} phosphor

3.1.1 Debye–Scherrer formula

An estimation of average crystalline size for the $Ca_2MgSi_2O_7:Eu^{2+}$, Dy^{3+} phosphor is done using Scherrer's formula; its mathematical representation as follows:

$$D = K\lambda/\beta Cos\theta \quad (2)$$

Where D is the crystalline size, K=0.94 (Scherrer constant), λ indicates the wavelength of incident X-ray (for Cu Kα radiation, λ = 1.5406 Å), β is the FWHM (Full width half maximum) of the peaks and θ is the corresponding Braggs diffraction angle [13, 17]. This phase structure are demonstrates akermanite type structure which belongs to the tetragonal crystal symmetry with space group $P\bar{4}2_1m$. This acquired structure is a member of the melilite group and forms a layered compound.

Table 1: According to prominent peak (211), position of the peak of the XRD patterns and the calculated value of parameters

No.	Parameters		$Ca_2MgSi_2O_7: Eu^{2+}, Dy^{3+}$
1	Crystal Structure		Tetragonal
2	Space Group		$P\bar{4}2_1m$
3	Lattice Parameters	a = 7.8071Å,	$a=\beta=y=90^0$
		b=7.8071Å,	
		c=4.9821Å	
4	Crystallite Size D(nm)		30.77nm
5	2θ [Deg]		31.24
6	Cell Volume		303.663 $(Å)^3$
7	Crystal Plane Spacing d (Å)		2.8630 (Å)
8	Strain		0.26

3.1.2 Strain determination by uniform deformation model (UDM)

The strain induced broadening in the powder material was calculated via the following formula given as below [13].

$$\varepsilon = \beta/4\tan\theta \quad (3)$$

3.2 FTIR Spectra

3.2.1 Functional group Discussion

Fig. 2 demonstrates the FTIR spectrum of phosphor. FTIR spectra were carried out in the range of (4000-400 cm^{-1}). This spectra revealed that the actual formation and evidence of functional group in phosphor. The band, centered at 473.46, 566.68, 648.80, 683.32, 738.32, 857.19, 947.32, 984.61 and 1045.43 cm^{-1} can be assigned to the presence of SiO_4 functional group. In the presented spectrum the absorption bands of silicate groups were clearly evident. The intense band allocated at 984.61 cm^{-1} was assigned to the Si-O-Si asymmetric stretch, the bands at 947.32 and 857.19 cm^{-1} to the Si-O symmetric stretch and the bands at 566.68 and 473.46 cm^{-1} to the Si-O-Si vibrational mode of bending. The band, allocated at 566.68, 648.80 and 1045.43 cm^{-1} can be assigned to the presence of SiO_4 group. Around 683.32 cm^{-1} in the prepared sample is the band due to Si-O bending vibrations [18-24].

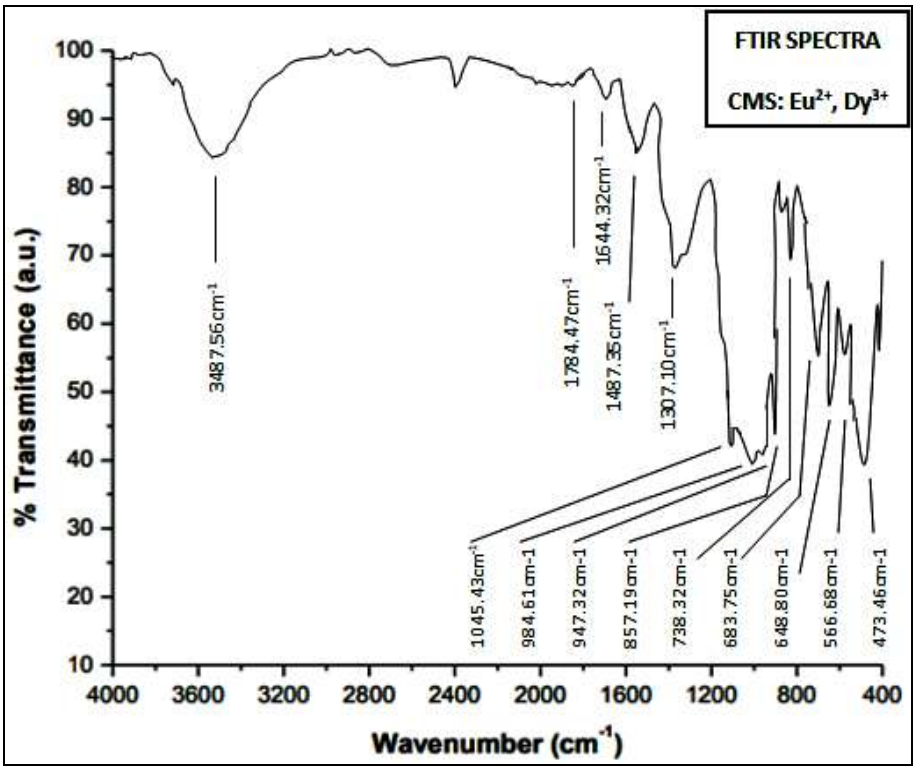

Fig 2: FTIR Spectra of $Ca_2MgSi_2O_7$: Eu^{2+}, Dy^{3+} Phosphor

According to Gou *et al.* [25] the absorption bands, posited at 1045.43, 984.61, and 566.68 cm^{-1}, respectively could be attributed to the evidence of SiO_4 group. Peak at 683.32 cm-1 may also be assigned to Ca-O bending vibrations and

there was shift of bands at 738.32 cm^{-1} are allocated to the vibration in the calcium [Ca^{2+}] ions. Mg-O bending is responsible for peak at 857.19 cm-1. The band allocated at 1784.47 cm-1 can be allocated to the presence of small amount of calcite. The free CO_3^{2-} ion has a D3h symmetry 69 (trigonal planar) and its spectrum is dominated by the band (asymmetric stretching) at 1644.32 cm^{-1}. The bands situated at 1784.47 and 1644.32 cm^{-1} are attributed to carbonation processes. Peak found at 1784.47 cm^{-1} can be attributed to Ca-O stretching. This might create distortion in the lattice resulting in 1307.10 and 1644.32 cm^{-1} vibration modes allocated to vibration in Ca^{2+} and Mg^{2+} ions respectively [25]. The evidence of carbonate bands is allocated to a carbonation process of the material as a consequence of the high calcite content in the synthesized phosphor [26].

3.3 Photoluminescence characteristics

3.3.1 Excitation and emission spectra

The excitation and emission spectra of $Ca_2MgSi_2O_7$: Eu^{2+}, Dy^{3+} phosphor prepared was shown in Figure 3. The excitation spectrum was monitored at a wavelength of 532 nm which shows prominent peak at 396 nm, respectively. The emission spectra are identical in shape and the bands differ only in intensities. The broadband emission spectra centered at 532 nm (Green region) observed under the ultraviolet excitation of 396 nm correspond to the Eu^{2+} emission arising due to transitions from sublevels of $4f^65d^1$ configuration to $^8S_{7/2}$ level of the $4f^7$ configuration but with Eu^{2+} occupying different lattice sites. Since the crystal field can greatly affect the $4f^65d^1$ electron states of Eu^{2+}, it suggests that the crystal field is not changed much with the compositional variation [28-30].

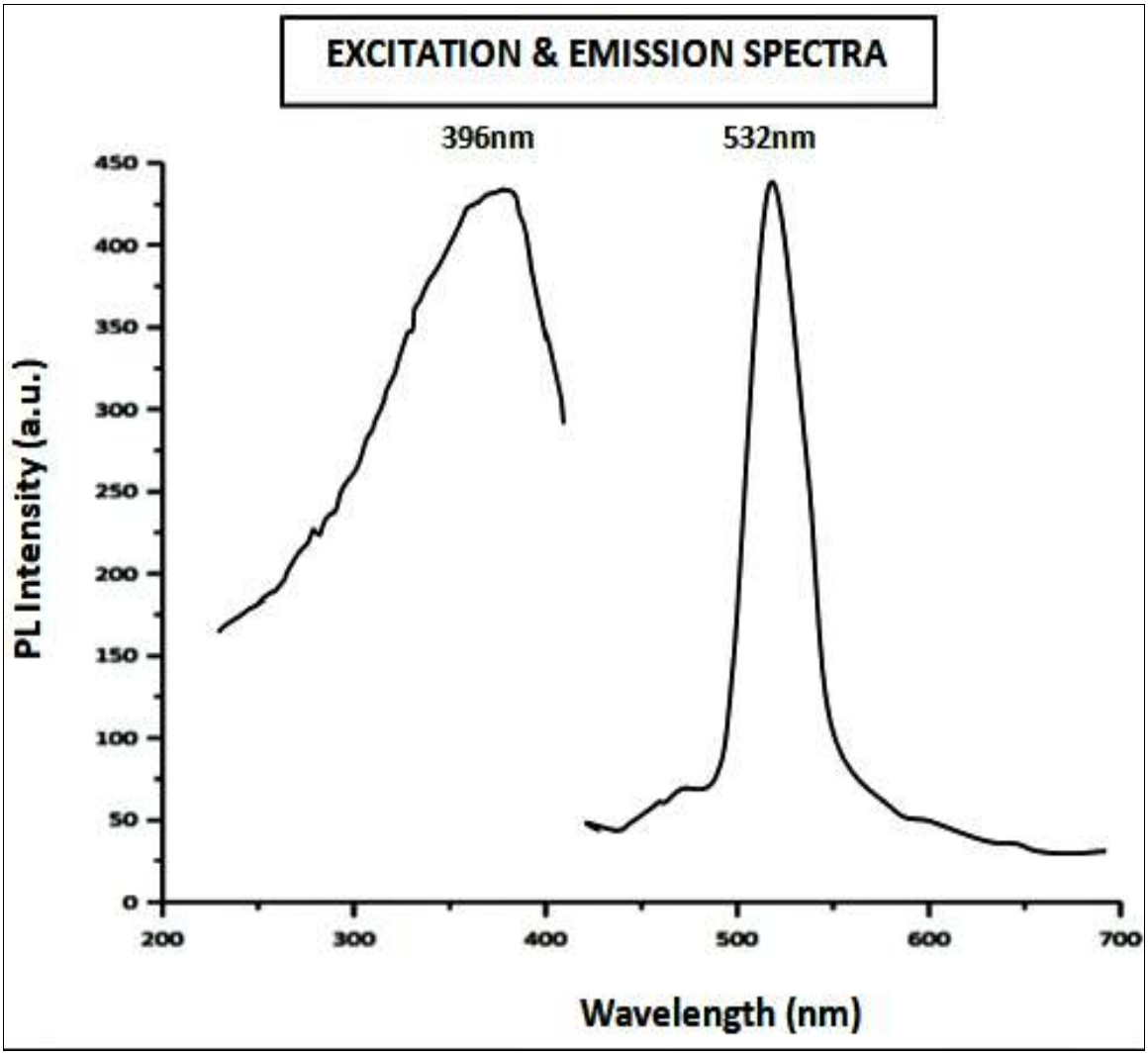

Fig 3: Excitation and Emission Spectra of $Ca_2MgSi_2O_7$: Eu^{2+}, Dy^{3+} Phosphor

Table 2: Concentrations of Rare Earths (In mol %)

Concentrations of Rare Earths (In mol %)		
Phosphor	**Eu^{2+}* (Doping)**	**Dy^{3+}* (Co-Doping)**
$Ca_2MgSi_2O_7$:Eu^{2+}, Dy^{3+}	0.5	2

3.4 CIE Chromaticity coordinate

CIE chromaticity diagram of this phosphor has been displayed in Fig. 4. In general case, color of any phosphor material is demonstrated through means of color coordinates. Color coordinates are one of the most significant factors for evaluating phosphors performance. The luminescence color of the samples excited under 396 nm has been characterized by the CIE chromaticity diagram. Luminescence colors of $Ca_2MgSi_2O_7$: Eu^{2+}, Dy^{3+} phosphor were placed in the bright green (x = 0.3174, y = 0.6692), corners. The chromatic co-ordinates of the luminescence of this phosphor are measure and reached to bright green luminescence [31].

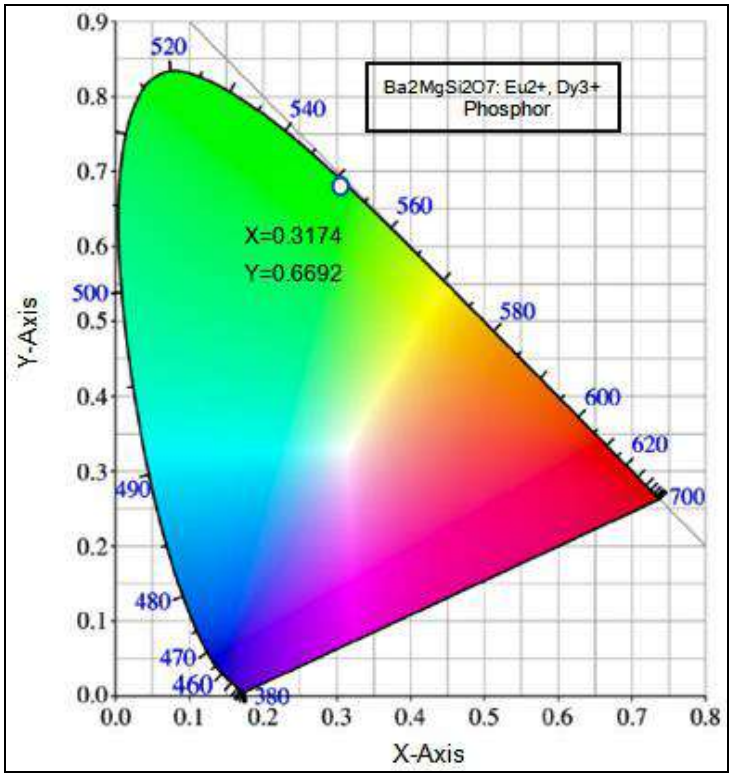

Fig 4: CIE Chromaticity Diagram

3.5 Thermo-luminescence properties

Fig: 7 displays TL glow curve of the sample for 15 min UV exposure. Thermo-luminescence signal is optimum for 15 minutes of UV exposure, after that it starts to decrease. The charge carrier density may have been increasing with increasing UV exposure, but after 15 minutes of UV exposure. Trap level may have started to destroy resulting in decrease in TL signals. The TL glow curves (Fig: 7) exhibit a broad peak because of the transition between ground and excited energy levels of the do-pant Eu^{2+}. The value of shape factor obtained between the ranges from 0.49-0.54, which signs the second order kinetics that supports the probability of retrapping released charge carriers before recombination. The afterglow of any phosphor is generated by the de-trapped carriers which recombine with the opposite carriers in the luminescent center with a transition resulting in visible region [32-33].

3.6 Calculation of kinetic parameters

Thermo-luminescence materials represent glow curves with one or more peaks, in case, when the charge carriers are liberated. The TL glow curve of a phosphor mainly depends on the kinetic parameters which include [Trap Depth or Activation Energy E], [Frequency Factor S] and [Order of Kinetics b]. There are various methods for determining the kinetic parameters from TL glow curves with the help of peak shape method [34-36].

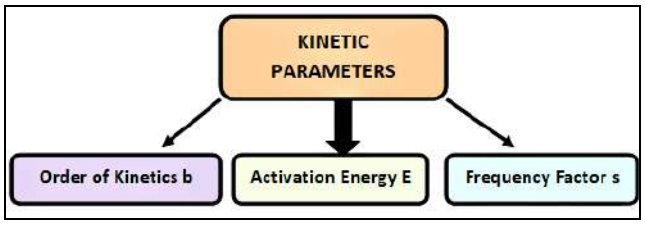

Fig 5: Types of Kinetic Parameters

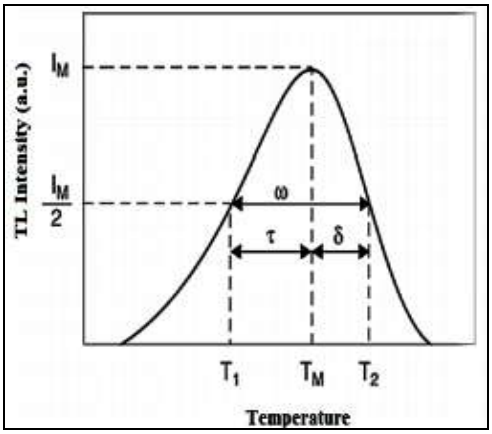

Fig 6: Schematic Diagram of Glow Curve Peak Shape Method

3.7 Order of Kinetics [b]

It is clearly depends on the peak shape of TL glow curve. The mechanism of recombination of de-trapped charge carriers with their counterparts is called as the order of kinetics [b]. The kinetic order for glow peak of this phosphor can be determined via calculating geometrical factor μ_g from the mathematical relation as follows:

$$\mu_g = \delta/\omega = T_2 - T_m/T_2 - T_1 \quad (4)$$

Where T_m is the optimum peak temperature, T_1 and T_2 are temperatures at half intensity on the ascending and descending parts of the glow peak, respectively [34-36].

Table 3: Order of Kinetics

Order of Kinetics	
First order kinetics	[μ_g = 0.39-0.42]
Second order kinetics	[μ_g = 0.49-0.52]
Mixed order kinetics	[μ_g = 0.43-0.48]

3.8 Activation Energy (E)

The activation energy [E] or trap depth can be determined by the general formula, which is valid for any kinetics. It is given by mathematical relation as follows:

$$E = C_\alpha \left(\frac{kT_m^2}{\alpha}\right) - b_\alpha (2kT_m) \quad (5)$$

Table 4: For general order kinetics, the values of the C_α and b_α ($\alpha = \tau, \delta, \omega$)

For general order kinetics, the values of the Ca and ba (a = T, 6, w)		
Fora = τ	Cτ = [1.51 + 3(μ_g - 4.2)	bτ = [1.58 + 0.42 (μ_g-0.42)]
Fora= δ	C_δ= [0.976 + 7.3(μ_g- 0.42)]	b_δ = 0
Fora = ω	C_ω, = [2.52 + 10.2(μ_g - 0.42)]	b_ω = 1

3.9 Frequency Factor (S)

After obtaining the order of kinetics [b] and activation energy [E], the frequency factor [S] can be determined with the help of the following mathematical relation through replacing the values of E and b:

$$\frac{\beta E}{kT_m^2} = s\left[1 + (b-1)\frac{2kT_m}{E}\right]\exp\left(-\frac{E}{kT_m}\right) \quad (6)$$

Where k is Boltzmann constant, E is activation energy, b is an order of kinetics, T_m is a temperature of peak position, and β is the heating rate. In the present work $\beta = 5\ ^oCs^{-1}$ [35-36].

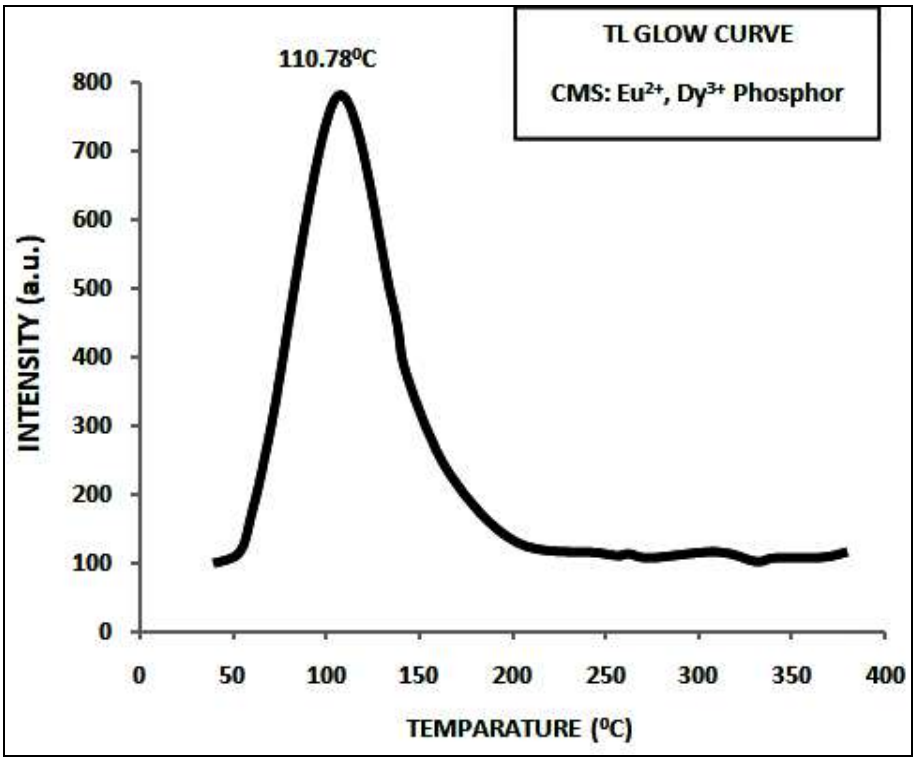

Fig 7: TL Glow Curve of $Ca_2MgSi_2O_7$:Eu^{2+}, Dy^{3+} Phosphor

Table 5: Kinetic Parameters

No.	Name of Phosphor	UV min	HTR	T_1 °C	T_m °C	T_2 °C	τ	δ	ω	$\mu = \delta/\omega$	E (eV)	Frequency Factor (s^{-1})
1.	CMS: Eu^{2+},Dy^{3+}	15	5	79.51	110.78	148.10	31.27	37.32	68.58	0.54	0.59	$8.55x10^7$

The shape factor, activation energy and frequency factor are also shown in Table: 4. Trap depth/Activation energy calculated as 0.59eV, which supports the fact that the sample show considerable amount of persistency in its luminescence property [37-39]. The TL glow curve, we find that the maximum glow curve is obtained at 110.78 °C. From 47.63 °C temperature observing, TL intensity is continuously increasing up to 110.78 °C, respectively. There after that the TL intensity is decreasing continuously up to 199.42 °C and their after TL intensity curve is near about flate and constant having the lowest value of TL intensity up to 400 °C. Sakai *et al.* and Mashangva *et al.* were reported that an appropriate trap depth (0.65-0.75 eV) is necessary for materials to display long persistence characteristics [39-40]. So, the trap density of synthesized materials is appropriate for long afterglow properties. In our case of phosphor, the geometric factor/ shape factor (μ_g) is obtained 0.54 (second order kinetics) and activation energy is found 0.59 eV respectively, which indicates of a considerable persistency.

4. Conclusion

$Ca_2MgSi_2O_7$:Eu^{2+}, Dy^{3+} phosphor was prepared via combustion synthesis route. The analysis of XRD patterns reveals the formation of single-phase crystal structure of the phosphor. The identified phase structure was tetragonal, akermanite structure with a space group $P\bar{4}2_1m$ which is confirmed through JCPDS # 77-1149. The average

crystallite size (D) is calculated as 30.77nm and lattice strain as 0.26 respectively. The actual phase formation and identification of functional group has been clarified with the help of FTIR spectroscopy. The broadband emission spectra centered at 532 nm (Green region) observed under the ultraviolet excitation of 396 nm correspond to the Eu^{2+} emission arising due to transitions from sublevels of $4f^6 5d^1$ configuration to $^8S_{7/2}$ level of the $4f^7$ configuration but with Eu^{2+} occupying different lattice sites. TL glow curve of this phosphor with 15min UV irradiation time at constant heating rate 5 $^oCs^{-1}$. The single TL glow curve peak was allocated at 110.78 ^oC temperature respectively, and these peak positions remains constant with UV irradiation time. The phosphors synthesized by combustion synthesis route which good supports the fact that the phosphor show considerable amount of persistency in its luminescence property.

5. Acknowledgements

We gratefully acknowledge the kind support for the facility of XRD analysis Dept. of Metallurgical Engineering and FTIR analysis Dept. of physics, NIT Raipur (C.G.). Authors are also thankful to Dept. of physics, Pt. Ravishankar Shukla University, Raipur (C.G.) for providing us the facility of Photoluminescence (PL) and Thermo-luminescence (TL) analysis. We are also heartily grateful to Dept. of physics, Dr. Radha Bai, Govt. Navin Girls College Mathpara Raipur (C.G.), providing the facility of muffle furnace and other essential research equipments.

6. Reference

1. McKeever S, Moscovitch M, Townsend P. Thermoluminescence Dosimetry Materials: Properties and Uses, Nuclear Tech. Pub., 1995.
2. Matasuzawa Xiu feng S, Xinran Z, Zhengfei P. J Mater Sci: Mater Electron 2009;20:433.
3. Blasse G, Wanmaker WL, Tervrugt JW *et al*. Philips. Res. Rep 1968;23:189.
4. Yamazaki K, Nakabayashi H, Kotera Y, Ueno A. J Electrochem, Soc 1986;133:657.
5. Sanjay Kumar Dubey, Shashank Sharma. A Brief Review to Study of Preparation and Photoluminescence (PL)Properties to Finding Possibilities of Divalent Europium Doped Barium Magnesium Silicate Based Phosphors, International Journal of Scientific Research and Engineering Development 2020, 3(3).
6. Erkul Karacaoglu, Bekir Karasu, Esra Ozturk. Advances in Science and Technology, Trans Tech Publications, Switzerland 2014;90:133-140.
7. Righini GC, Ferrari M. Photoluminescence of rare-earth-doped glasses Rivista Del Nuovo Cimento 2005, 28(12). DOI 10.1393/ncr/i2006-10010-8.
8. Lin L, Yin M, Shi CS, Zhang WP. Luminescence properties of a new red long-lasting phosphor: Mg_2SiO_4:Dy^{3+}, Mn^{2+}, J Alloys Compd. 2008; 455:327-330.
9. Rao TGVM, Rupesh Kumar A, Veeraiah N, Rami Reddy M. Optical and structural investigation of Sm^{3+}–Nd^{3+} co-doped in magnesium lead borosilicate glasses, J Phys. Chem. Solid 2013;74:410-417.
10. Matsuzawa T, Aoki Y, Takeuchi N *et al*., J Electronchem. Soc. 1996;143:26-70.
11. JIA W, Yuan H, Lu L, Liu H, Yen WM, Lumin J. 1998;76:424.
12. Kingsely JJ, Patil KC. Material letters 1988;6:427.
13. Sharma S, Dubey SK, Diwakar AK, Pandey S. Novel white light emitting ($Ca_2MgSi_2O_7$:Dy^{3+}) Phosphor. Journal of Materials Science Research and Reviews 2021;8(4):164-171.
14. Shashank Sharma, Sanjay Kumar Dubey, Sanjay Pandey, Diwakar AK. Optical Characteristics of Novel WLED ($Ca_2MgSi_2O_7$:Dy^{3+}) Phosphor. North Asian International Research Journal of sciences, Engineering & I.T 2021, 7(11).
15. (Joint Committee on Powder Diffraction Standard) JCPDS file No. 77-1149.
16. Data Base Code AMCSD 0008032.
17. Ubale AU, Sangawar VS, Kulkarni DK. Size dependent optical characteristics of chemically deposited nanostructured ZnS thin films. Bulletin of Materials Science 2007;30(2):147-51.
18. Shannon RD. Revised effective ionic radii and systematic studies of interatomic distances in halides and chalcogenides. Acta crystallographica section A: crystal physics, diffraction, theoretical and general crystallography 1976;32(5):751-67.
19. Qin Fei C, Chang D, Mao J Alloy. Compd 2005;390(1-2):134-137.
20. Frost RL, Bouzaid JM, Reddy BJ. Vibrational spectroscopy of the sorosilicate mineral hemimorphite $Zn_4(OH)_2Si_2O_7 \cdot H_2O$. Polyhedron 2007;26(12):2405-12.
21. Chandrappa GT, Ghosh S, Patil KC. Synthesis and Properties of Willemite, Zn_2SiO_4, and M^{2+}:Zn_2SiO_4 (M= Co and Ni). Journal of Materials Synthesis and Processing 1999;7(5):273-9.
22. Makreski G, Jovanovski B, Kaitner A, Gajovic T. Biljan, Vib. Spectrosc 2007;44:162.
23. Caracas R, Gonze X. Ab initio determination of the ground-state properties of $Ca_2MgSi_2O_7$ åkermanite. Physical Review B 2003;68(18):184-102.
24. Salim MA, Hussain R, Abdullah MS, Abdullah S, Alias NS, Ahmad Fuzi SA *et al*., Solid State Sci. Technol 2009;17(2):59-64.
25. Gou Z, Chang J, Zhai W. J Eur. Ceram. Soc 2005;25:1507-1514.
26. Martinez A, Izquierdo-Barba I, Vallet-Regi M. Chem. Mater 2000;12:3080-3088.
27. Jiang L, Chang C, Mao D, Feng C. J Mater. Sc. & Engg. B 2003;103:271-275.
28. Wu H, Hu Y, Zeng B, Mou Z, Deng L. J Phy. Chem. Sol 2011;72:1284-1289.
29. Shi C, Fu Y, Liu B, Zhang G, Chen Y, Qi Z *et al*., 2007, 122-123, 11-13.
30. Lin L, Zhonghua Z, Weiping Z, Zhiquing Z, Min Y. J Rare Earths 2009;27(5):749-752.
31. CIE. International Commission on Illumination. Publication CIE no. 15 (E-1.3.1) 1931.
32. Chen T, McKeever S. Theory of Thermo-luminescence and Related Phenomena World Scientific Publishing Co. Pvt. Ltd. 1997.
33. Kaur J, Shrivastava R, Dubey V, Jaykumar B. Res. Chem. Intermed., DOI 10.1007/s11164-013-1112-5 2012.
34. Shashank Sharma, Sanjay Kumar Dubey, Diwakar AK. Thermo-luminescence properties of Host $Ca_2MgSi_2O_7$ Phosphor. IRJMETS 2021, 3(11).
35. Chen R, Mckeever SWS. Theory of Thermo-luminescence and Related Phenomenon, World Scientific Press, Singapore 1997.

36. Mckeever SWS. Thermo-luminescence of Solids, Cambridge University Press, Cambridge 1985.
37. Blasse G, Grabmair BC. Luminescent materials, Springer-Verlag 1994.
38. Pagonis V, Kitis G, Furetta C. Numerical and Practical Exercises in Thermoluminescence, Springer Science+ Business Media, Inc 2006.
39. Mashangva M, Singh MN, Singh B. Indian J Pure Appl. Phys 2011;49:583-589.
40. Sakai R, Katsumata T, Komuro S, Morikawa T, Lumin J 1999;85:149-154.